A Comparison of a Wide-Slot and a Stacked Patch Antenna for the Purpose of Breast Cancer Detection

David Gibbins, Maciej Klemm, Ian J. Craddock, Jack A. Leendertz, Alan Preece, and Ralph Benjamin

***Abstract*—A wide-slot UWB antenna is presented for intended use in the detection scheme being developed at the University of Bristol, based on the principle of synthetically focused UWB radar using a fully populated static array. The antenna's measured and simulated, input and radiation characteristics are presented and compared to an existing, stacked patch antenna that has been designed for the same purpose. The results of this study show that the wide-slot antenna has excellent performance across the required frequency range. Compared to the stacked-patch antenna used in our previous array, the wide-slot antenna can be 3 times smaller (in terms of front surface). The compact nature of the slot antenna means that the detection array can be densely populated. Additionally, this new antenna offers better radiation coverage of the breast. For angles up to 60° away from bore-sight radiated pulses are almost identical (fidelity >95%), whereas for the patch antenna fidelity falls to 58% at the angular extremes. This uniform radiation into the breast should result in focused images with low levels of clutter.**

***Index Terms*—Breast cancer, microwave radar, ultrawideband (UWB) antennas.**

I. Introduction

BREAST cancer is the most common form of cancer in women (excluding skin cancers) [1], [2] however with early detection there is a high chance of successful treatment and long-term survival. The most common method in use for the detection of breast cancer is X-ray mammography and, while it has been an effective tool for detecting breast cancer it is recognized that the technique has a number of limitations including producing a significant number of false-negative and false-positive results [3], [4].

Microwave imaging has gained interest recently due to advances in both hardware and imaging software. The method is a potential alternative imaging technique that would be inexpensive, provide more sensitive 3D imaging data, avoid using ionising radiation and would yield a system that is both quick and comfortable for the patient [5]. Microwave imaging technology relies on there being a detectable difference in the dielectric properties of a tumor and the surrounding breast tissue at microwave frequencies, such that when the breast is illuminated with microwave radiation there is a significant reflection from the tumor [6]. Early work in this area was based on the premise that the structure of the breast is relatively electrically homogeneous and that a contrast of approximately 5:1 exists between malignant and normal tissue [7], [8]. More recent studies [9] have shown that, while the contrast between malignant and normal adipose-dominated tissue could be as large as 1:10, the contrast in denser glandular tissue is much less at around 10%. This presents a significantly more challenging problem than was initially thought and serves to underline the need for an antenna design with the best possible performance in terms of bandwidth, size and pattern characteristics.

There are a number of techniques under investigation utilizing microwave signals as a means of detection. One approach considers it as an inverse scattering problem (microwave tomography [10]), in which the breast is illuminated with microwave radiation and the scattered energy is received at a number of remote locations. From this information the permittivity distribution inside the breast may be estimated. However the data processing required when implementing this method is complex and it is not easy to see how information from many different frequencies may be included [11].

An alternative approach is to tackle the problem using a similar architecture to that of ground penetrating radar (GPR) in an approach first introduced independently by Hagness *et al.* [12] and Benjamin [13], [14]. Ultrawideband (UWB) radar imaging as a means of detecting breast cancer, is a technique that is currently being developed by a number of research teams [12], [15], [16]. In these systems a short pulse, or a synthesized pulse constructed from a frequency sweep, is directed into the breast and the reflected signals are then detected by one or more receive antennas. The sweep is transmitted in turn from a number of different locations and the resulting set of received signals are then time- or phase-shifted and added in order to enhance returns from high contrast objects and to reduce clutter. Such radar-based systems are capable of producing high resolution images without the need for complicated reconstruction algorithms, due to the wideband nature of the UWB signals. With this approach there is a trade-off between simplicity of analysis and information, since—unlike the inverse scattering approach—material properties are not directly recovered [16].

A critical part of any detection scheme is the antenna design. In order to obtain high resolution, accurate images the antennas must be able to radiate signals over a wide band of frequencies while maintaining the fidelity of the waveform over a large angular range [17]. If the antenna is to be used in a fully populated array aperture (as at Bristol) then there is an additional, quite

Manuscript received January 13, 2009; revised June 11, 2009. First published December 28, 2009; current version published March 03, 2010. This work was supported by the EPSRC and Micrima Ltd.

The authors are with the Centre for Communications Research, Department of Electrical and Electronic Engineering, University of Bristol, Bristol BS8 1UB, U.K. (e-mail: david.gibbins@bristol.ac.uk; m.klemm@bristol.ac.uk; ian.craddock@bristol.ac.uk; j.leendertz@bristol.ac.uk; a.w.preece@bristol.ac.uk; R.Benjamin@bristol.ac.uk).

Color versions of one or more of the figures in this paper are available online at http://ieeexplore.ieee.org.

Digital Object Identifier 10.1109/TAP.2009.2039296

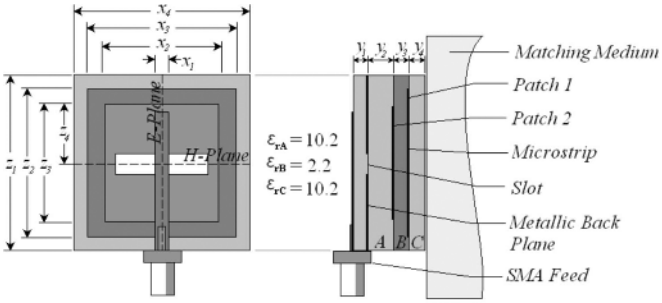

Fig. 1. Schematic of the stacked patch antenna (not to scale).

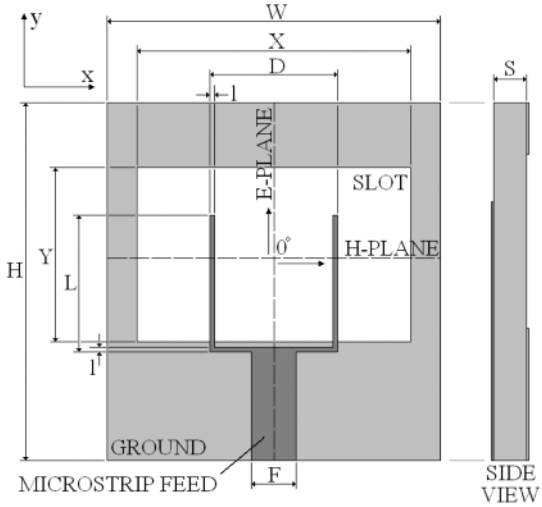

Fig. 2. Schematic of the wide-slot antenna (not to scale).

critical, geometrical size constraint placed on the antenna; the antenna's geometrical dimensions must be as small as possible in order that the maximum number of antennas may accommodated in the array. This will allow as much information to be gathered as is possible which, in turn, will reduce clutter in the results.

Existing antenna designs either use resistive loading to improve their UWB performance, e.g., resistively loaded monopoles [18], dipoles [16], [19], [20], bowtie [21], [22], and horn [23] antennas, which result in low efficiencies [6], or antennas are unsatisfactorily large, e.g., stacked patch [24] and planar monopole [25], all of which have dimensions in the order of 25 mm or greater while operating in the same frequency band. This paper presents a new slot antenna designed for use in Bristol's breast cancer detection system. The dimensions of the slot, feed and ground have been chosen so that the antenna operates optimally while cavity-backed, with the slot in contact with a matching medium that has electrical properties similar to that of normal breast tissue. In terms of it's electrical size, this antenna has frontal surface area of aproximately half that of the planar monopole in [25] and a third of that of the stacked patch.

The structure of this paper is as follows; firstly the new wide-slot antenna will be presented along with a slot-fed, stacked patch antenna that was previously designed for the same application [24]. The performance of the patch will be compared with that of the wide-slot antenna. The method by which measurements were obtained will then be discussed and the paper will then go on to present results obtained by measurement and FDTD computer simulation. These will include return-loss, transfer functions, fidelity and time domain characteristics.

II. The Antennas and Experimental Setup

The antennas being examined in this paper are:

(i) A cavity backed version of a stacked patch antenna (Fig. 1) that has been previously designed at the University of Bristol. This antenna was designed for use in the breast cancer detection system being developed at that institution and was originally presented in [24].

(ii) A fork-fed wide-slot antenna (Fig. 2) that is intended to replace the stacked patch antenna in this application.

Both these antennas are in the main constructed of dielectric substrates with a high relative permittivity of 10.2. They have been optimized to operate with the antenna face immersed in a matching medium with dielectric properties similar to that of human breast tissue, in order to reduce reflections by eliminating the air/skin interface [6]. The matching medium used is described in [26] and is mainly comprised of oil of paraffin and distilled water. This mixture has a relative permittivity of around between 9 and 10 at frequencies between 2 and 10 GHz and an attenuation of 2 dB/cm at a frequency of 8 GHz As this material has been designed to have similar electrical properties to human breast fat it is also used as a simple breast phantom for the antenna measurements presented in this paper.

A. The Stacked Patch

The stacked patch antenna consists of a microstrip line feeding a slot, which in turn excites an arrangement of stacked patches. The slot feed was used in order to eliminate the inductance associated with a probe feed. The patches sandwich a lower permittivity substrate and their size was chosen so that a lowest order resonance was achieved at either end of the desired frequency band. The dimensions were then manually optimized by using an FDTD computer simulation [24]. The efficiency of this antenna was found from FDTD to be 88% at 4 GHz, and 97% at 6 and 8 GHz (these values were found by simulation since experimentally obtaining full 3D radiation patterns of the antenna is difficult when submerged in the medium). The stacked patch antenna can be seen in (Fig. 1); the dimensions (in [mm]) being: $x_1 = 0.66$, $x_2 = 6$, $x_3 = 9$, $x_4 = 18$, $y_1 = 0.64$, $y_2 = 1.9$, $y_3 = 0.8$, $y_4 = 1.27$, $z_1 = 18$, $z_2 = 6.5$, $z_3 = 6$, $z_4 = 3$. It should be noted that this figure shows the antenna without the cavity used to back the antenna while taking measurements.

B. The Wide Slot

The wide-slot antenna consists of an approximately square slot set in a ground plane on one side of a substrate with a relative permittivity of 10.2. On the other side of the substrate is a forked microstrip feed that splits, just below the slot, from a 50 Ω feed into two 100 Ω sections which excite the slot. The fork feed was chosen as a means of increasing the operational bandwidth [27]. As with the patch the efficiency of this antenna has been found by simulation. At 3 GHz the efficiency was calculated as 60%,

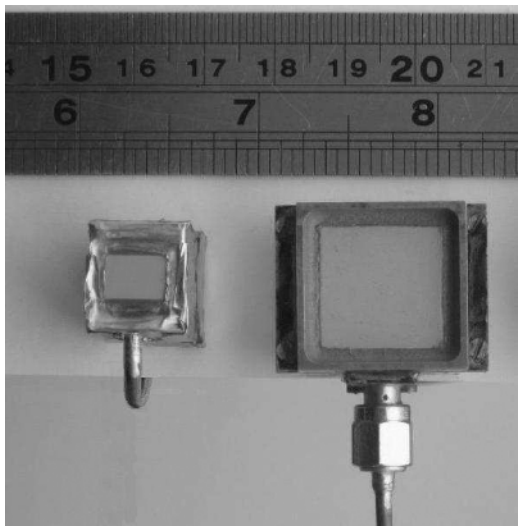

Fig. 3. The wide-slot antenna with a prototype cavity, fed directly from a coaxial cable (left). The SMA fed stacked patch antenna mounted in the cavity used for the measurements (right).

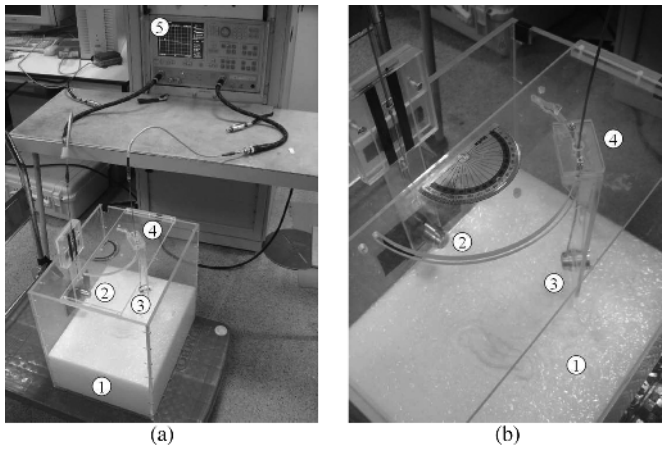

Fig. 4. (a) Experimental arrangement. (b) Close-up of positioning apparatus.

at 6 GHz at 80% and 90% at 9 GHz. The new antenna can be seen in (Fig. 2), its dimensions are: $\mathrm{H} = 14$, $\mathrm{Y} = 7$, $\mathrm{L} = 6.5$, $\mathrm{D} = 4$, $\mathrm{W} = 13$, $\mathrm{X} = 10$, $\mathrm{F} = 1.25$, $\mathrm{S} = 1.25$, $\mathrm{l} = 2$ (all dimensions in [mm]).

This antenna is based on that described in [27] but has been heavily modified and optimized to work efficiently when the slot is in contact with a matching medium with relative permittivity of approximately 10. This optimization was a manual iterative procedure performed using FDTD simulations and included the resizing and rescaling of the slot, fork feed and ground plane and the introduction of the high permittivity substrate on which the current antenna is built.

The simulations used in the optimization process were run using FDTD software developed at the University of Bristol. In the simulation the slot side of the antenna radiates into a 50 mm-thick block of dielectric ($\sigma = 0$, $\epsilon = 9$) with an air gap behind the antenna. The meshes used in the optimization process have cells of sizes varying from 1 to 0.1 mm, while number of cells in the mesh varied from $178 \times 51 \times 186$ to $203 \times 134 \times 210$ cells depending on the stage of the optimization. The workspace was terminated by Mur 1st order absorbing boundary conditions. A planar current source between the ground and microstrip was used to excite the feed line with a raised cosine pulse of width 112 ps. The transmission line was terminated inside the workspace using a vertical 50 Ω resistive load.

Both antennas were designed to work with a cavity attached to the rear side where the microstrip feed is located. This was done to prevent any radiation from the back surface of each antenna coupling into other antennas in the array. The cavities used consist of an absorber lined, brass enclosure that extends down to the face of the antenna.

The two antennas are shown together in Fig. 3. This figure clearly demonstrates the difference in size between them. It should be noted that, while a detailed description is not in the scope of this article, the feed for the wide-slot has been modified to eliminate the SMA connector and, hence, further reduce the overall dimensions. This was done by connecting the feed coaxial cable directly to the antenna itself. A hole was made in the side wall of the cavity level with the top surface of the antenna substrate and the microstrip line. The outer conductor of the coaxial cable was soldered to the edges of the hole which was just large enough for the inner conductor and dielectric insulator to pass through. Inside the cavity the dielectric is terminated at the edge of the antenna substrate and the inner conductor is soldered to the top surface of the microstrip line.

C. Experimental Setup

In order to fully characterize the antennas the input and radiation characteristics must be determined. As these results are required with the antennas radiating into a breast phantom, obtaining measurements, especially the radiation data, is quite a challenge. Since it is the transmission performance between two of the antennas that is the critical factor in the imaging application and due to a lack of suitable reference antenna, the radiation characteristics of the antenna under test were found by measuring the transmission between two identical antennas of that type.

The experimental setup used to take measurements can be seen in Fig. 4. In this arrangement both receiving and transmitting antennas are immersed in a large tank of the matching medium/phantom, described at the start of Section II (1). The transmitting antenna (2) is fixed close to the tank wall in a stationary position facing out into the medium. The receiving antenna (3) is mounted on a rig (4) that describes an arc of radius 100 mm around a central point at which is the center of the face of the first antenna. The manner in which the second rig follows the arc results in the second antenna always directly facing the first. Measurements were taken in the E and H planes using a VNA (5), the chosen plane selected by attaching the antennas to the measurement rig in the correct orientation before immersion in the phantom medium.

III. Results

It is important that the input and radiation characteristics of the antenna be known across the whole of the antennas intended operational bandwidth and angular range. As the antenna is intended to radiate a simulated short pulse its transient response

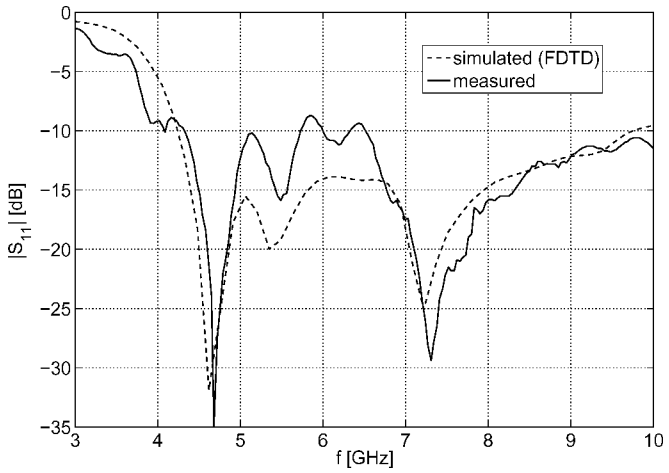

Fig. 5. Measured and simulated (FDTD) S_{11} characteristics of the wide-slot antenna.

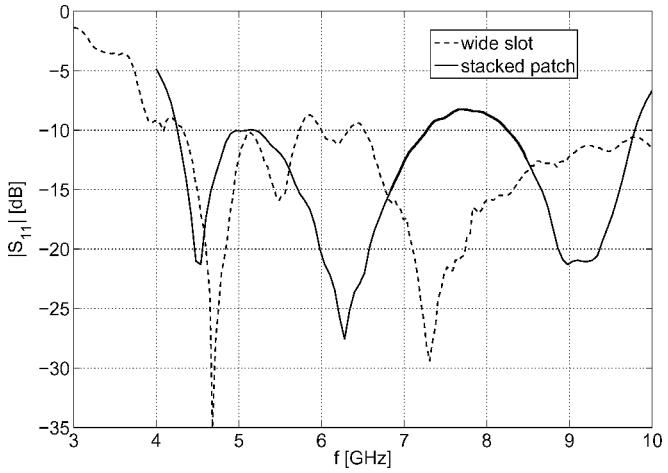

Fig. 6. Comparison of measured S_{11} characteristics for the wide slot and patch antennas.

is also important, including the fidelity of the signals that the antenna transmits.

A. Input Response

The simulated reflection coefficient for the cavity backed wide-slot antenna can be seen in Fig. 5, along with the equivalent measured results. It can be seen that there is a pleasing level of agreement between the two data sets. Both show that the -10 dB bandwidth extends from around 4 GHz (4.5 GHz in the simulated case) to above 10 GHz which is sufficient for this application. In the measured data there are some small discrepancies where the S_{11} rises above -10 dB around 6 GHz. This frequency region will be examined later to assess its impact on the transmission response. Both simulated and measured results show that there are two major nulls in the response and are in good agreement in their location in the frequency spectrum. The differences between the two plots are probably due to fabrication tolerances particularly the feed, which has dimensions of the order of 0.2 mm. This level of agreement gives confidence that other results obtained using the FDTD model will correctly reflect the true properties of the antenna. The FDTD model used to produce these results had the same setup as that used in the optimization process. The workspace was $50 \times 83.25 \times 49$ mm and was descretized using a mesh made up from $203 \times 134 \times 210$ cells with sizes varying from 1-0.1 mm.

When the measured return loss of the new wide-slot antenna is compared with that of the stacked patch (Fig. 6) it can be seen that the two antennas show comparable performance characteristics, with similar -10 dB bandwidths; the patch demonstrating a 5.5 GHz–10 dB bandwidth between 4.25 and 9.75 GHz. The patch antenna data also shows a drop in performance across the frequency range of interest between 7.3 and 8.3 GHz where the S_{11} rises to -8 dB at it's maximum. This discrepancy will also be examined in the transmission response.

B. Transmission Response

In order to achieve minimal distortion to UWB signals transmitted into the breast, it is desirable that the magnitude of the transfer function of the antenna be as flat as possible across the required frequency range [28]. Examining the measured bore-sight S_{21} in Fig. 7 (bore-sight being normal to the plane of the antennas—see Fig. 1, Fig. 2) shows that both antennas have approximately the same performance; both having a maximum magnitude around 4 GHz which then drops steadily with frequency.

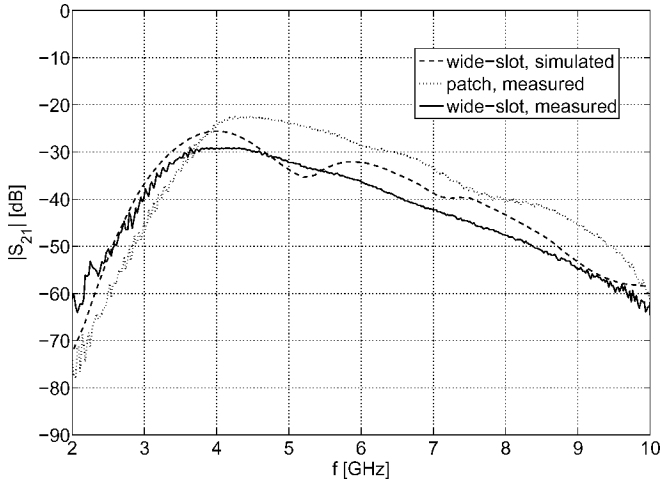

Fig. 7. Simulated and measured S_{21} characteristics (bore-sight direction) for the wide slot and patch antennas.

The major difference is that the stacked patch has a transfer function magnitude that is consistently 7 dB higher from 4–9 GHz. This is because the main beam of the patch antenna is narrower than that of the wide-slot, concentrating the radiated energy at bore-sight, in other words, the patch has a higher gain due to its larger aperture. This can be illustrated by employing an approximation based on beamwidths to find the directivity at bore-sight $[D_0]$ of both antennas at a particular frequency. Assuming that each antenna only has one main lobe the directivity at 4.5 GHz, in dBs is given by [29];

$$D_0 = 10 \log \left(\frac{41253}{\theta_{1r} \cdot \theta_{2r}} \right). \quad (1)$$

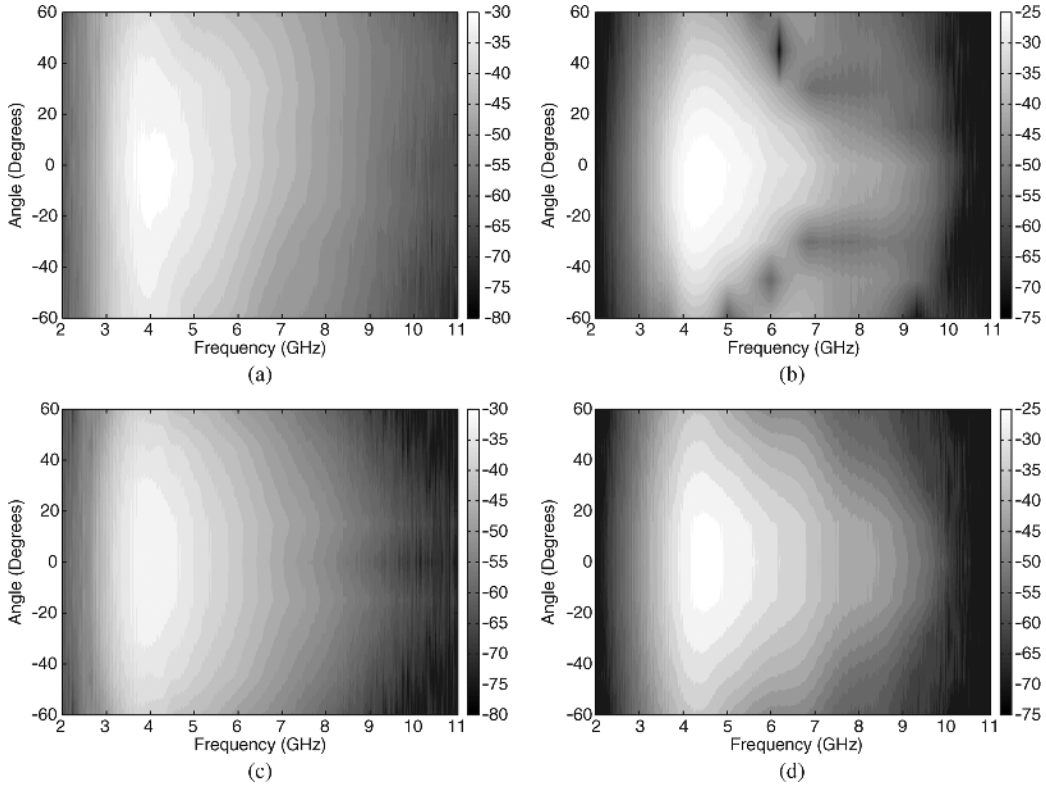

Fig. 8. Measured S_{21} data: (a) E-plane, wide-slot antenna; (b) E-plane, stacked patch antenna; (c) H-plane, wide-slot antenna; (d) H-plane, stacked patch antenna. Angle 0° corresponds to the bore-sight radiation direction.

Where θ_{1r} and θ_{2r} are the 3 dB beamwidths in degrees for two orthogonal planes (in this case the E and H-planes). Substituting the beamwidth values for the patch and slot gives

$$D_{0slot} = 10\log\left(\frac{41253}{74^\circ \cdot 78^\circ}\right) = 8.5\ \text{dB} \tag{2}$$

$$D_{0patch} = 10\log\left(\frac{41253}{54^\circ \cdot 64^\circ}\right) = 10.8\ \text{dB}. \tag{3}$$

Hence, the gain would be approximately 2.3 dB less for the wide-slot antenna than for the patch. The transfer functions in Fig. 7 are measured using two antennas, therefore for one antenna the wide-slot's gain is 3.5 dB lower than that of the patch. Comparing this value to the 2.3 dB difference due to the change in aperture it can be seen that the lower directivity of the wide-slot accounts for the majority of this difference; the remaining 1.2 dB is most likely due to slightly higher back-radiation from the slot or to measurement errors. The wider antenna beam (hence, lower gain) seen in the results for the slot is in fact desirable, since it gives the most uniform illumination of the breast by the antenna array elements, the reduction in bore-sight gain is simply an unavoidable consequence of this.

The main reason for the shape of the slope of the measured responses is the attenuation in the matching medium, which increases with frequency. This is borne out in the fact that the simulated S_{21} for the wide-slot antenna was practically flat before losses in the phantom were taken into account. With their inclusion (post simulation using a frequency dependent model) the simulated results again show a good agreement with those

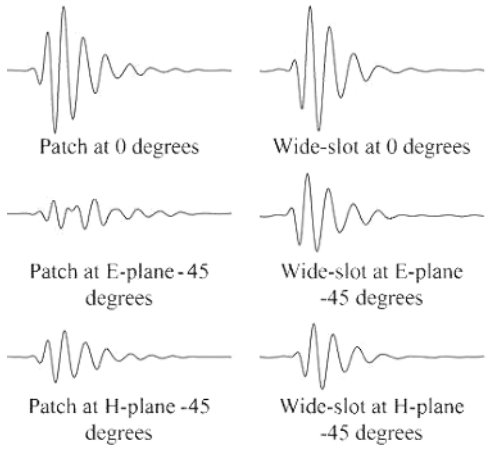

Fig. 9. Examples of pulses synthesized from measured transfer functions normalized to the maximum field strength at 0°. Each pulse is displayed in a 2 ns time window.

measured. The simulated S_{21} was also found, using an FDTD model with the same general setup and antenna mesh as that used to measure the s11 but with two antennas facing each other through a block of the high dielectric medium, 100 mm thick.

Referring back to the issues raised with the S_{11} data the wide-slot antenna seems to have been affected very little by the slight mismatch in the 6 GHz region. The stacked patch does show a slight dip in the transfer function at around 7–8 GHz indicating that in this case the mismatch may be having an effect.

Examining only the bore-sight gain gives a limited view of the antenna's performance. For our application it is required that

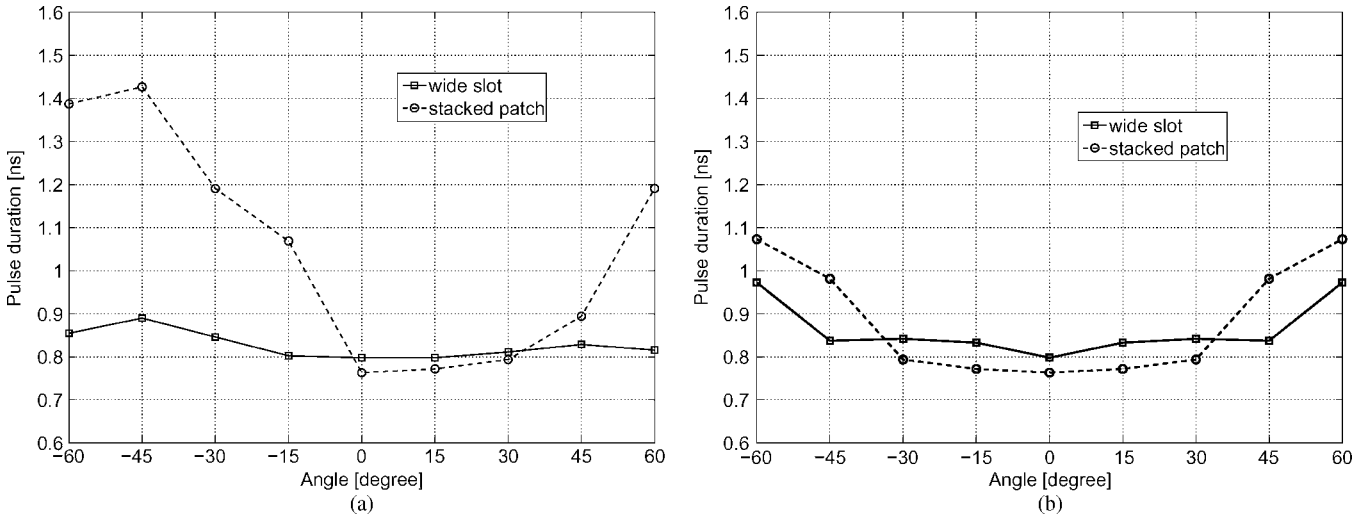

Fig. 10. Comparison of measured pulses' duration (99% of pulse energy): (a) E-plane, (b) H-plane.

the antenna has as uniform a response as possible from $+60°$ to $-60°$ away from bore-sight, in both the E and H-planes (the E-plane being in the y-direction—see Figs. 1 and 2). In order to best understand what is happening at a variety of angles and frequencies Fig. 8 illustrates how the transfer function data from 2–11 GHz varies from $+60°$ to $-60°$, while the contour lines indicate signal magnitude in 2 dB steps.

Examining the E-plane plots shows that the wide-slot antenna [Fig. 8(a)] maintains its signal strength across the angular range. The antenna has maximum field strength at 0° but never drops below 10 dB of this value. The variation in the magnitude with frequency is similar at all angles. There does seem to be a slight squint in the positive direction at higher frequencies, which is probably a result of the lack of symmetry in this plane due to the location of the feed on the slot's lower edge. This squint is minimal, manifesting itself as a 3–5 dB difference between values at the angular extremes. Fig. 8(b) shows the equivalent results for the patch. This shows that the main beam of the patch antenna is narrow in comparison and above 7 GHz splits into a number of lobes which vary by up to 25 dB between the nulls and peaks in only 30°. The drop off of signal magnitude at higher frequencies noted in the bore-sight transfer functions (Fig. 7) can again be seen between 9 and 10 GHz, with the addition that at more extreme angles this occurs at lower frequencies. The asymmetries in the E-plane S_{21} of the patch (and as will be seen later, pulse duration data) are related and likely due to the feed. The microstrip/slot feed arrangement means that the fields exciting the patches are not symmetrical in the E-plane (a similar effect can also be seen in the form of the squint in the wide-slot radiation characteristics in this plane). These asymmetries in the field feeding the patches lead to asymmetries in the radiated fields.

Examining the equivalent H-plane results [Fig. 8(c) and (d)] shows that, as would be expected, the plots are symmetrical due to the fact that the antennas are also symmetrical in this plane. Both antennas show a broad, relatively consistent beam-width across the frequency range. It should be noted that, as in the E-plane, the wide-slot antenna shows a flatter response across frequency and angular ranges, the beam width of the patch becoming narrower at higher frequencies.

C. Pulse Duration

For radar-based breast cancer detection it is important that pulses produced by the antenna (or in this case synthesised from a frequency sweep) are as short as possible with minimal late-time ringing [12]. Therefore pulse duration is a good indication of the ability of the antenna to effectively transmit UWB signals into the medium. To test this the measured frequency domain S_{21} data for the transmission between two antenna elements was obtained from the VNA. Pulses were then synthesized by applying a pulse template to this transfer function. Some examples of received pulses can be seen in Fig. 9, while a detailed description of the time and frequency domain responses of the template pulse can be seen in [30].

The time taken for 99% of the energy of these pulses to be received was then calculated. This process was carried out in the E and H-planes at an angular resolution of 15° from $+60°$ to $-60°$ and results are presented in Fig. 10. Pulse durations for the E-plane [Fig. 10(a)] show that, as in the S_{21} plots, there is an asymmetry present for both antennas. The performance of the wide-slot shows in general that the pulses produced by this antenna are shorter and there is far less variation with angle (0.8–0.9 ns) than those produced by the patch (0.75–1.45 ns). This can be seen in the example pulses (Fig. 9) where there is little difference at bore-sight but at $-45°$ there is significantly more late-time ringing in the pulse produced by the patch.

Examining the equivalent H-plane data [Fig. 10(b)] shows that the wide-slot antenna maintains a pulse width of just above 0.8 ns in the range of $+/-45°$, this rises to a value of 0.97 ns at the angular extremes. The patch antenna shows a marginally better performance than the wide-slot between the angles $+/-30°$, with a pulse duration of just below 0.8 ns. Beyond these angles the length of the pulses increases to 0.98 ns at $+/-45°$ and 1.07 ns at $+/-45°$. This difference is illustrated in Fig. 9 where, although not as marked as in the E-plane there is still evidence of late-time ringing. The difference in the performance of the two antennas is the result of the poorer transmission properties of the patch antenna at high angular values

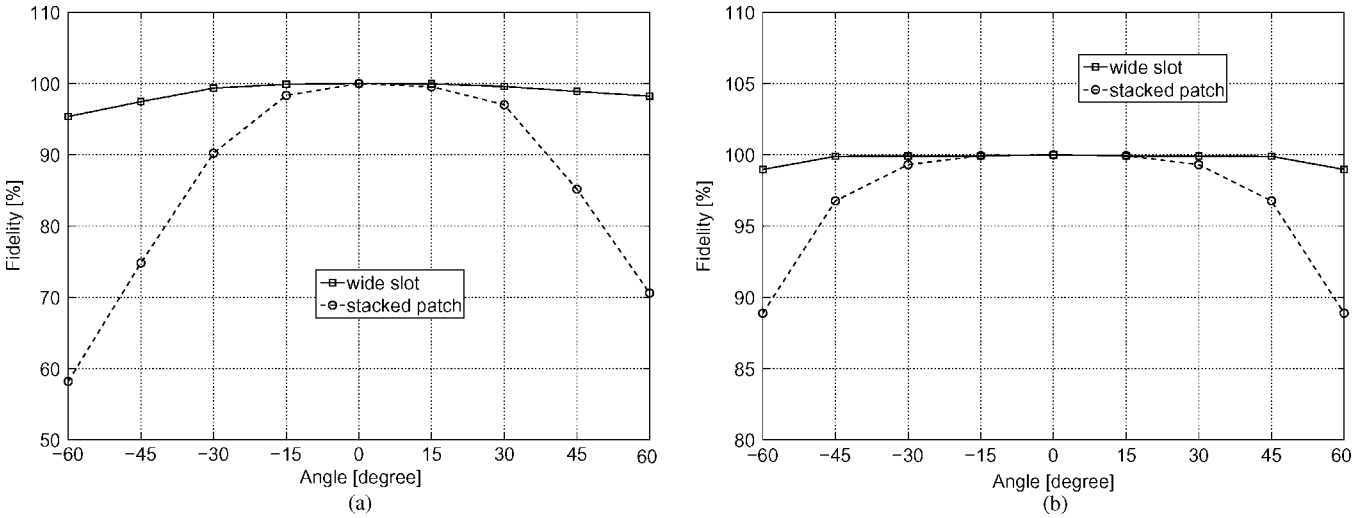

Fig. 11. Comparison of measured fidelities: (a) E-plane, (b) H-plane.

[Fig. 8(d)] when compared to the equivalent transmission characteristics for the wide-slot [Fig. 8(c)] which are much more similar to those at bore-sight.

D. Fidelity

In order to study the level of distortion in the radiated pulses the fidelity of the signals was computed at the same points for which pulse duration was found. The fidelity is the maximum magnitude of the cross correlation between the normalized observed response and an ideal response [28] which in this case is the signal radiated at bore-sight. The fidelity, F, is given by

$$F = \max \frac{\int_{-\infty}^{\infty} x(t) \cdot y(t-\tau) dt}{\sqrt{\int_{-\infty}^{\infty} |x(t)^2| \, dt \cdot \int_{-\infty}^{\infty} |y(t)^2| \, dt}}. \tag{4}$$

The fidelity parameter, F, is the maximum of the cross-correlation function and compares only shapes of both waveforms, not amplitudes. The calculated fidelity for the antennas in the E-plane can be seen in Fig. 11(a). The asymmetry noted previously can again be seen in both sets of results. The fidelity of the signals transmitted by the wide-slot antenna is excellent and fidelity remains above 95% for the entire angular range. Near bore-sight the performance of the patch is good, however beyond angles of $+/-20°$ the fidelity drops dramatically. This distortion is due to the irregularities seen in the transfer function data and borne out in the pulse duration measurements. The distortion at larger angles can be seen in Fig. 9 when the pulses at $-45°$ are compared. The wide-slot antenna reproduces the signal at bore-sight with reasonable accuracy at this angle whereas the pulse produced by the patch shows significant distortion.

For the H-plane [Fig. 11(b)] both antennas perform well, with the fidelity remaining above 90% for almost the entire angular range; the fidelity of signals radiated from the wide-slot never dropping below 98%. Once again the stacked patch performance degrades at high angles. This drop in performance can also be related back to the transfer function data and is most likely due to the rapid drop off seen in the signal content at higher frequencies, subsequent ringing (seen in the lengthening pulse duration) and signal distortion that occurs at these higher angles.

IV. Radar Detection Experiment

A numerical experiment has been conducted to demonstrate the suitability of the wide-slot antenna for the imaging application. The experiment consists of transmitting a UWB pulse into a numerical breast phantom to locate a tumor-like inclusion. The FDTD experimental setup uses the same excitation arrangement, boundary conditions and is based on the same mesh structure as the simulations used to obtain the antenna's S-parameters. Two antennas are spaced 65 mm apart. Antenna 1 radiates a pulse and reflected signals are received by Antenna 2. The dielectric properties of the numerical phantom are ($\sigma = 0.2$, $\epsilon_r = 9$). A 5 mm diameter spherical inclusion is positioned in the phantom. The relative permittivity of the inclusion is set at 50 giving a contrast of 5:1 with the background medium, similar to the contrast that might be seen between a tumor and adipose breast tissue [9]. The position of the inclusion is varied between $+/-60°$, at 10° intervals, along an arc located mid-way between the two antennas as shown in Fig. 12.

The simulated coupling between the antenna elements is around 60 to -80 dB. In the detection system the coupling between antennas is obviously dependent on their location in the array. However this issue is not critical as any signals directly coupling between antennas are removed prior to the signal analysis by calibration. For details of the calibration process and more information on the coupling between elements in a previous prototype of the array see [30].

As the signal received at Antenna 2 contains reflections and coupling between the antennas, as well as the response from the inclusion, a calibration is performed to remove these unwanted signals. The calibration signal is obtained by running simulation without an inclusion present. This background signal is subtracted from the signal that is received with the inclusion present, leaving only the response from the target, allowing the effect of the antenna to be clearly seen.

As the path length is the same for each inclusion, waveforms from the different inclusion positions, normalized to their maximum value, can be added coherently to produce an aggregate pulse that summarizes the antenna performance over the entire

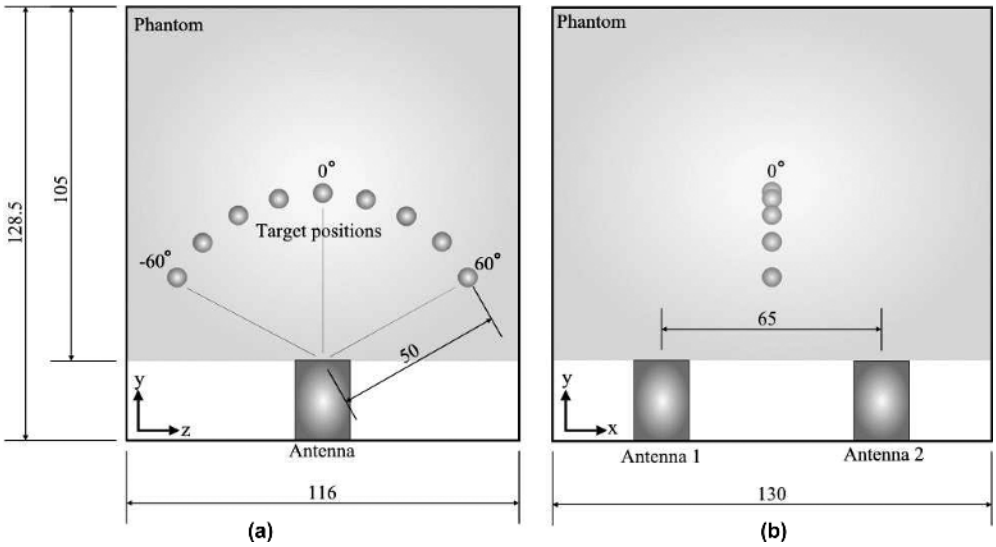

Fig. 12. Schematic of the (a) y-z plane and (b) the y-x plane of the FDTD model used in the radar detection experiments (all dimensions in mm).

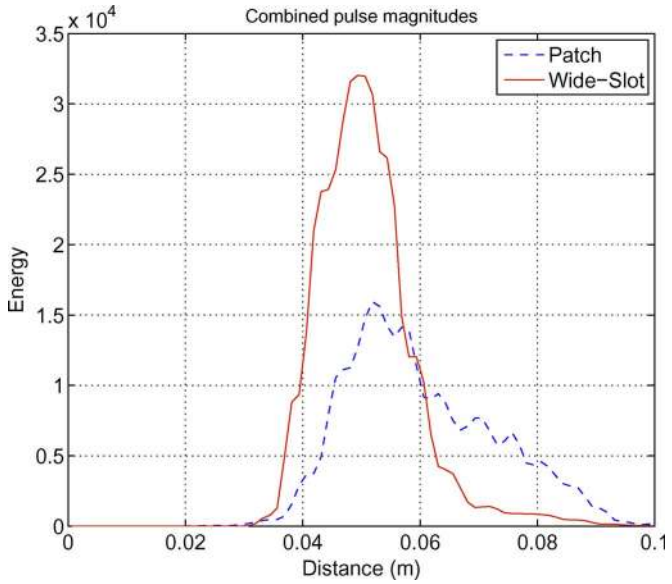

Fig. 13. Integrated spatial energy on a radial path outwards from the centre of the inclusion arc.

angular range. Squaring and then integrating this pulse over a sliding window corresponding to the transmit pulse width yields an energy curve that can be calibrated to show the radial distance of the inclusion from the centre of the arc Fig. 13 The curve should peak at the true position of 5 cm.

The results of this analysis show that the energy distribution for the wide-slot response has a single peak exactly centred at the radial location of the inclusion. The peak has a width-at-half-height of just over 15.6 mm, allowing the position of the inclusion to be easily identified. In comparison the energy distribution produced by the patch response is much more diffuse with a lower, less well-defined peak and a width-at-half-height of 26.3 mm, nearly twice that of the slot antenna. This is a result of the increased distortion and dispersion of pulses produced by the stacked patch at angles away from boresight. From these results it can be concluded that the wide-slot would be a good candidate for use in a radar-based breast imaging system.

V. Conclusion

A wide-slot antenna intended for use in a UWB antenna array for breast cancer detection system has been presented and compared to a stacked patch antenna that was previously designed for the same application. Return loss measurements showed that both antennas had suitable bandwidths for use in a UWB detection system and good agreement was found between simulated and measured results for the wide-slot antenna. On examination of the transmission properties it was found that, while the stacked patch performed well at angles close to bore-sight, at wider angles of illumination (which are very important in this application) the transfer function showed significant degradation which manifested itself as significant late-time ringing and distortion of transmitted signals. This was especially notable in the E-plane.

The wide-slot antenna performed well over the entire angular/frequency range and faithfully radiated pulses at angles up to 60° away from bore-sight. This was confirmed by results from a simple radar detection experiment that showed that the wide slot performed well in breast imaging scenario. This, along with the fact that the antenna is approximately half the size of existing antenna designs, suggests that it is an excellent candidate for use in a UWB radar breast cancer detection system

Acknowledgment

The authors would like to acknowledge K. Stevens for help with the manufacture of the measurement setup and Prof. J. P. McGeehan for the provision of facilities at the Centre for Communications Research, University of Bristol.

References

[1] B. C. Cancer Agency [Online]. Available: http://www.buccancer.bc.ca
[2] J. Ferlay, F. Bray, P. Pisani, and D. Parkin, *Globocan 2000: Cancer Incidence, Mortality and Prevalence Worldwide*. : IARC CancerBase, 2001, Version 1.0(5).

[3] J. G. Elmore and M. B. Barton *et al.*, "Ten year risk of false positive screening mammograms and clinical examinations," *New England J. Med.*, vol. 338, no. 16, pp. 1089–1096.
[4] P. T. Huynh and A. M. Jarolimek, "The false-negative mammogram," *Radiograph*, vol. 18, no. 5, pp. 1137–1154, 1998.
[5] E. Fear, S. C. Hagness, P. Meaney, M. Okoniewski, and M. Stuchly, "Enhancing breast tumor detection with near-field imaging," *IEEE Microw. Mag.*, vol. 3, no. 1, pp. 48–56, Mar. 2002.
[6] , B. Allen and M. Dohler, Eds. *et al., Ultra-Wideband Antennas and Propagation for Communications, Radar and Imaging*. Chichester, U.K.: Wiley, 2007.
[7] A. J. Surowiec, S. S. Stuchly, J. R. Barr, and A. Swarup, "Dielectric properties of breast carcinoma and the surrounding tissues," *IEEE Trans. Biomed. Eng.*, vol. 35, no. 4, pp. 257–263, April 1988.
[8] W. T. Joines, Y. Zhang, C. Li, and R. L. Jirtle, "The measured electrical properties of normal and malignant human tissues from 50 to 900 MHz," *Med. Phys.*, vol. 21, p. 547, 1994.
[9] M. Lazebnik *et al.*, "A large-scale study of the ultrawideband microwave dielectric properties of normal, benign and malignant breast tissues obtained from cancer surgeries," *Phys. Med. Biol.*, vol. 52, p. 6093, 2007.
[10] P. M. Meaney, M. W. Fanning, D. Li, S. P. Poplack, and K. D. Paulsen, "A clinical prototype for active microwave imaging of the breast," *IEEE Trans. Microw. Theory Tech.*, vol. 48, no. 11, pt. 1, pp. 1841–1853, Nov. 2000.
[11] Q. Fang, P. M. Meaney, and K. D. Paulsen, "Microwave image reconstruction of tissue property dispersion characteristics utilizing multiple-frequency information," *IEEE Trans. Microw. Theory Tech.*, vol. 52, no. 8, pt. 2, pp. 1866–1875, Aug. 2004.
[12] S. C. Hagness, A. Taflove, and J. E. Bridges, "Two-dimensional FDTD analysis of a pulsed microwave confocal system for breast cancer detection: Fixed-focus and antenna-array sensors," *IEEE Trans. Biomed. Eng.*, vol. 45, no. 12, pp. 1470–1479, Dec. 1998.
[13] R. Benjamin, "Detecting Reflective Object in Reflective Medium," U.K. patent GB2313969, Dec. 10, 1997.
[14] R. Benjamin, "Synthetic, post-reception focusing in near-field radar," in *Proc. EUREL Int. Conf. (Conf. Publ. No. 431) The Detection of Abandoned Land Mines: A Humanitarian Imperative Seeking a Technical Solution*, Oct. 7–9, 1996, pp. 133–137.
[15] I. J. Craddock, R. Nilavalan, J. Leendertz, A. Preece, and R. Benjamin, "Experimental investigation of real aperture synthetically organised radar for breast cancer detection," in *Proc. IEEE Antennas and Propagation Society Int. Symp.*, 2005, vol. 1B, pp. 179–182, vol. 1B.
[16] E. C. Fear and M. A. Stuchly, "Microwave detection of breast cancer," *IEEE Trans. Microw. Theory Tech.*, vol. 48, no. 11, pt. 1, pp. 1854–1863, Nov. 2000.
[17] C. J. Shannon, E. C. Fear, and M. Okoniewski, "Dielectric-filled slotline bowtie antenna for breast cancer detection," *Electron. Lett.*, vol. 41, no. 7, pp. 388–390, Mar. 31, 2005.
[18] J. M. Sill and E. C. Fear, "Tissue sensing adaptive radar for breast cancer detection-experimental investigation of simple tumor models," *IEEE Trans. Microw. Theory Tech.*, vol. 53, no. 11, pp. 3312–3319, Nov. 2005.
[19] M. Fernández Pantoja, S. González García, M. A. Hernández-López, A. Rubio Bretones, and R. Gómez Martín, "Design of an ultra-broadband V antenna for microwave detection of breast tumors," *Microw. Opt. Technol. Lett.*, vol. 34, no. 3, pp. 164–166, Aug. 5, 2002.
[20] H. Kanj *et al.*, "A novel ultra-compact broadband antenna for microwave breast tumor detection," *Prog. Electromagn. Res.*, vol. 86, pp. 169–198, 2008.
[21] S. C. Hagness, A. Taflove, and J. E. Bridges, "Three-dimensional FDTD analysis of a pulsed microwave confocal system for breast cancer detection: Design of an antenna-array element," *IEEE Trans. Antennas Propag.*, vol. 47, no. 5, pp. 783–791, May 1999.
[22] H. Kanj and M. Popovic, "T- and X-arrangement of "dark eyes" antennas for microwave sensing array," in *Proc. IEEE Proc. Antennas and Propagation Society Int. Symp.*, Jul. 9–14, 2006, pp. 1111–1114.
[23] X. Li, S. C. Hagness, M. K. Choi, and D. W. van der Weide, "Numerical and experimental investigation of an ultrawideband ridged pyramidal horn antenna with curved launching plane for pulse radiation," *IEEE Antennas Wireless Propag. Lett.*, vol. 2, no. 1, pp. 259–262, 2003.
[24] R. Nilavalan and I. J. Craddock *et al.*, "Wideband microstrip patch antenna design for breast cancer detection," *IET Microw. Propag.*, vol. 1, no. 2, pp. 277–281, 2007.
[25] H. M. Jafari *et al.*, "A study of ultrawideband antennas for near-field imaging," *IEEE Trans. Antennas Propag.*, vol. 55, no. 4, pp. 1184–1188, Apr. 2007.
[26] J. Leendertz, A. Preece, R. Nilavalan, I. J. Craddock, and R. Benjamin, "A liquid phantom medium for microwave breast imaging," presented at the 6th Int. Congress of the Eur. Bioelectromagnetics Assoc., Budapest, Hungary, Nov. 2003.
[27] J.-Y. Sze and K.-L. Wong, "Bandwidth enhancement of a microstrip-line-fed printed wide-slot antenna," *IEEE Trans. Antennas Propag.*, vol. 49, p. 1020-102, Jul. 2001.
[28] D. Lamensdorf and L. Susman, "Baseband-pulse-antenna techniques," *IEEE Antennas Propag. Mag.*, vol. 36, no. 1, pp. 20–30, Feb. 1994.
[29] C. A. Balanis, *Antenna Theory*, 3rd ed. Hoboken, NJ: Wiley, 2005.
[30] M. Klemm, I. J. Craddock, A. Preece, J. Leendertz, and R. Benjamin, "Evaluation of a hemi-spherical wideband antenna array for breast cancer imaging," *Radio Sci.*, vol. 43, 2008.

David Gibbins received the M.Eng. degree (first class honors) in aerospace engineering from Liverpool University, Liverpool, U.K., in 2004.

He joined the University of Bristol, Bristol, U.K., in 2005 where he is working toward the Ph.D. degree and is a Research Assistant in the Centre for Communications Research where he is a member of Bristol's Breast Cancer Imaging Project. His involvement in this project includes UWB antenna design, FDTD electromagnetic simulation and inverse scattering. His other research interests include conformal FDTD meshing techniques and applications of UWB radar.

Maciej Klemm was born in 1978. He received the M.Sc. degree in microwave engineering from Gdansk University of Technology, Poland, in 2002 and the Ph.D. degree from the Swiss Federal Institute of Technology (ETH) Zurich, Switzerland, in 2006.

In February 2003, he joined the Electronics Laboratory, Swiss Federal Institute of Technology (ETH) Zurich, Switzerland. At ETH his research interests included small UWB antennas and UWB communications, antenna interactions with a human body, electromagnetic simulations, microwave MCM technologies and millimeter-wave integrated passives (European IST LIPS project). In spring 2004, he was a Visiting Researcher at the Antennas and Propagation Laboratory, University of Aalborg, Denmark, where he was working on the new antennas for UWB radios. In February 2006, he joined the University of Bristol (UoB), Bristol, U.K., where he currently holds a position of a Research Associate. At UoB, he is working on the microwave breast cancer detection and UWB textile antennas. His involvement in the breast cancer project includes antenna design, electromagnetic modeling, experimental testing as well as participating in clinical trial.

Dr. Klemm received the Young Scientists Award at the IEEE MIKON 2004 Conference for his paper, "Antennas for UWB Wearable Radios." For his paper, "Novel Directional UWB Antennas" he won the CST University Publication Award competition in 2006. In 2007, he won the "Set for Britain" competition for the top early-career research engineer and received a Gold Medal at the House of Commons.

Ian J. Craddock is a Reader in the CCR, University of Bristol, Bristol, U.K. His research interests include antenna design, electromagnetics, biomedical imaging and radar, funded by organizations such as EPSRC, QinetiQ, DSTL and Nortel. He leads Bristol's Breast Cancer Imaging Project, this project winning the IET's Innovation in Electronics prize in 2006. He has published over 100 papers in refereed journals and proceedings. He has led a workpackage on ground-penetrating radar in an EU Network of Excellence and has a related active research interest in antennas and propagation for instrumentation within the human body. He has delivered numerous invited papers to conferences in Europe, the US and Asia and chaired sessions at leading international conferences.

Jack A. Leendertz received the B.Sc. degree in physics with mathematics from Bristol University, Bristol, U.K.

He is with the Centre for Communications Research, Department of Electrical and Electronic Engineering, University of Bristol. His interests include microwave engineering, coherent optics in engineering, instrumentation for medical research and microwave imaging.

Alan Preece is a Clinical Scientist and Emeritus Professor of Medical Physics at Bristol University, Bristol, U.K., who previously researched biological effects of ionizing and non-ionizing radiation on humans. Current work is applied to practical equipment design and the clinical application of microwave imaging in human subjects for the purpose of identifying and evaluating the imaging possibilities of such microwaves in detection of breast cancer.

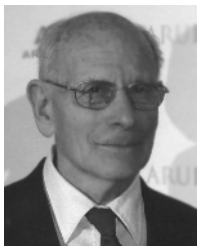

Ralph Benjamin received the B.Sc. degree (1st class honors) in electronic engineering from Imperial College, U.K., and invented the single-sideband mixer during his undergraduate course.

He joined RN Scientific Service in 1944 and developed first countermeasure resistant 3D radar, and first force-wide integrated CCIS (Command, Control, Communications and Intelligence System) from 1947 to 1957. In 1947, he patented the interlaced cursor, controlled by joy-stick or mouse, to link displays to stored digital information. He also patented the world's digital compression of video data, and first digital data link, 1947, still in use NATO-wide as "Link 11". Following repeated "special merit" promotions, Head of Research and Deputy Director, Admiralty Surface Weapons Establishment, 1961–64. (Evening/night work to lay the theoretical foundations for this field resulted in a Ph.D., then published as the textbook on *Signal Processing*) 1961 Acting International Chairman NATO "Von Karman" studies on "Man and Machine" and "Command and Control." In the 1950s and 1960s, leading member of DTI Advanced Computer Techniques Project. Chief Scientist Admiralty Underwater Weapons Establishment (AUWE), 1964 to 1971, combined with Director, AUWE, and MoD Director Underwater Weapons R&D (and member of Navy Weapons Department Board), 1965 to 1971. (Published personal contributions led to the London D.Sc.) Chief Scientist, Chief Engineer and Superintending Director, GCHQ 1971 to 1982. This entailed responsibility for fast-track research, development, procurement, and deployment and use of equipment and techniques for the collection interpretation evaluation and assessment of Electronic or Signals Intelligence information. (Most projects had to create urgent solutions to problems which the opposition's leading experts thought they had made impossible.) From 1972 to 1982, his functions were combined with those of Chief Scientific Advisor to both the Security Service and SIS, and with acting as Cabinet Office Co-ordinator, Intelligence R&D. Also, Visiting Professor, University of Surrey for two 3-year terms, 1972 to 1978, during which time he helped to start the Surrey University mini-satellite program. Following his first "retirement", Head of Communications Techniques and Networks and semi-official global research coordinator NATO (SHAPE Tech Centre) 1982 to 1987. Graduate NATO Staff College, 1983. Currently, he is a Visiting Research Professor at University College, London, U.K. and Bristol University, Bristol, U.K. Until recently, he was also a Visiting Professor at Imperial College, London, External Ph.D. Supervisor at Open University, and external Post-Graduate Course Examiner, Military College of Science, Member of Court, Brunel University. During all these appointments, he combined the administration of large scientific/engineering organizations and of their R&D programmes, with creative, innovative up-front leadership, as illustrated by numerous classified and learned-society publications and patents.